

Article

# The Effects of Reduction and Thermal Treatment on the Recrystallization and Crystallographic Texture Evolution of 5182 Aluminum Alloy

Sofia Papadopoulou <sup>1,2,\*</sup>, Athina Kontopoulou <sup>2</sup> , Evangelos Gavalas <sup>1,2</sup>   
and Spyros Papaefthymiou <sup>2</sup> 

<sup>1</sup> ELKEME S.A., 61st km Athens-Lamia Nat. Road, 32011 Oinofyta, Viotia, Greece; egavalas@elkeme.vionet.gr

<sup>2</sup> Laboratory of Physical Metallurgy, School of Mining & Metallurgical Engineering, Division of Metallurgy and Materials, National Technical University of Athens, 9, Her. Polytechniou str., Zografos, 15780 Athens, Greece; ath.kontopoulou@gmail.com (A.K.); spapaef@metal.ntua.gr (S.P.)

\* Correspondence: spapadopoulou@elkeme.vionet.gr; Tel.: +30-2262-60-4309

Received: 17 September 2020; Accepted: 15 October 2020; Published: 16 October 2020



**Abstract:** During forming, thickness reduction and thermal treatment affect the recrystallization and evolution of the crystallographic texture of metallic materials. The present study focuses on the consequences of rolling reduction of a widespread aluminum alloy with numerous automotive, marine and general-purpose applications, namely Al 5182. Emphasis is laid on the crystallographic texture and mechanical properties on both hot and cold-rolled semi-final products. In particular, a 2.8 mm-thick hot-rolled product was examined in the as-received condition, while two cold-rolled sheets, one 1.33 mm and the other 0.214 mm thick, both originating from the 2.8 mm material, were examined in both as-received and annealed (350 °C for 1 h) conditions. Electron back-scatter diffraction indicated the presence of a large percentage of random texture as well as a weak recrystallization texture for the hot-rolled product, whereas in the case of cold rolling the evolution of  $\beta$ -fiber texture was noted. In addition, tensile tests showed that both the anisotropy as well as the mechanical properties of the cold-rolled properties improved after annealing, being comparable to hot-rolled ones.

**Keywords:** DC Casting; 5182 alloy; crystallographic texture; hot rolling; cold rolling; crystallographic components; microstructural evolution; aluminum

## 1. Introduction

The need for lightweight, recyclable, malleable and strong materials has led to the use of aluminum alloys for a constantly increasing spectrum of industries with emphasis on the transportation sector both on land and sea serving automotive and marine applications, but also the food industry [1,2]. To gain tailored properties to match the needs of these industries various rolling and heat treatment processes must be fully controlled in order to tailor the microstructure, to enable an enhanced forming ability, and to gain expected final mechanical properties. In particular, the evolution of the crystallographic texture throughout forming and heat-treating stages, with regard to the final mechanical properties, is of great importance [3]. Liu et al. have examined the effect of direct casting (DC) versus continuous (CC) casting of Al 5052 exhibiting the effect of the casting process on the texture [4], while Yu et al. studied similar phenomena on Al 5182 [5]. Crystallographic texture is affected at every step of the thermomechanical procedure [6,7]. Therefore, the correlation between crucial process parameters (e.g., temperature, alloy composition, casting procedure, number of reduction steps etc.) and their influence to texture evolution are paramount for the optimization of the desired properties through the relevant steps.

The 5182 Al alloy (see Table 1) suits applications such as the beverage can lid as well as automotive structural parts and inner body parts [8–11]. Hot and cold rolling are used to match the final gauge. The more intense plastic deformation is applied to the alloy, the more the microstructure is affected. In the conventional rolling process, on the surface of the Al sheet that is produced, the shear stresses that are present lead to higher local strain. This results in more fine grains on the surface than in the middle of the produced sheet [12]. Concerning the effect of cold rolling on Al alloys, crystallographic components that consist the  $\beta$  fiber (brass, copper and S) are expected. Cold rolling is characterized by the activation of octahedral slip systems while hot rolling has the tendency to provoke the slip of non-octahedral systems. At the stacking fault energy is attributed the way that the plastic deformation will occur (slip and/or twinning). The Al alloys are plastically deformed through slip on the systems  $\{111\} \langle 110 \rangle$  [13]. The texture components could be categorized in (i) rolling texture components (Copper, Dillamore or Taylor, S, Brass), (ii) shear texture components (rot-Cube<sub>ND</sub>,  $\gamma$  fiber,  $\alpha$  fiber Inverse brass, E, F,) and (iii) recrystallization texture components (Cube, P, R and Goss) [14–19].

The amount of recrystallization components that will be formed during the production process depends on the prior deformed state. The aim is to obtain the desired equally balanced amount of texture components in order to achieve the best formability through the control of the earing behavior [17–19].

Two main theories had been widely discussed in the scientific community regarding texture evolution, the orientation of (i) the nucleation and (ii) the growth. Cube oriented grains are those that combine characteristics from the two theories altogether; they tend to grow from remained Cube bands and they tend to be favorable points for the growth of deformation crystallographic components [20]. The more intense effect on cube oriented grains is given by the rolling reduction percentage, the annealing conditions and the chemistry of the alloy [21]. It is crucial to decrease the presence of Cube component by controlling the hot rolling process, since a high amount of cube-oriented grains could lead to reduced drawability [16].

In general, cold rolling induces work hardening resulting in an increase of both yield strength and hardness. The application of heat-treatment (annealing), however, can reduce the extent of these effects, [14,15] and, in addition, it may reduce anisotropy. K. J. Kim et al. [16] studied the feasibility of deep drawing for aluminum alloys 5182 after annealing at 350 °C for different durations and concluded that the sheet, which had been annealed for 20 min exhibited the best drawability. The best combination of crystallographic components, according to the authors, to obtain the optimal drawability is  $\gamma$  fiber ND// $\langle 111 \rangle$  and rot-Cube<sub>ND</sub>  $\{001\} \langle 110 \rangle$ . Due to the thermal losses during the insertion of the samples, however, other researchers considered a treatment time of one hour [22–26]. It has been documented that the rolling process results in the formation of a  $\beta$  fiber texture [27], consisting of the Cu $\{112\} \langle 111 \rangle$ , S $\{123\} \langle 634 \rangle$  and brass $\{110\} \langle 112 \rangle$  components. In addition, the application of heat treatment results in a further transformation of the grains into cube  $\{001\} \langle 100 \rangle$ , P  $\{011\} \langle 1-11 \rangle$ , Q  $\{013\} \langle 3-31 \rangle$ , R  $\{132\} \langle 4-21 \rangle$  and Goss  $\{011\} \langle 100 \rangle$  components [14]. The crystallographic component R  $\{124\} \langle 211 \rangle$  is similar to the crystallographic component S  $\{123\} \langle 634 \rangle$ . Beck and Hu [28] pointed out that the R orientation can originate from the deformation texture by two different mechanisms. The first mechanism is the retained R from the rolling texture, where the stored dislocation energy is being reduced partially through extended recovery reactions, named as continuous recrystallization in the relevant literature. The second mechanism is about the forming of grains exhibiting R orientation genuinely via discontinuous recrystallization by the growth of nuclei into S oriented grains at the grain boundaries of the deformed bands and subsequent growth under the depletion of the rolling components, B, C and S. An R orientation is created through discontinuous recrystallization by the procedures of nucleation and growth, contrary to the display of a notable swiftness regarding the corresponding rolling texture, which is apparent to the ODFs with large scattering close to the R component. During discontinuous recrystallization the R component competes with the cube orientation with regard to nucleation. Since the R grains can grow up to substantial volume fractions due to the high amount of potential nucleation sites, they can outweigh the cube orientation [29].

Each texture component causes the material to form “ears” at different directions from RD (Cu, S and brass components results into the formation of 45° “ears” in deep drawn cups while the cube component strengthens the presence of 90° “ears”); hence to minimize earing, a proper combination of texture components should be obtained [17,29]. It is reported by O. Engler et al. [13] that transient orientations along the deformation process from the recrystallization towards the rolling texture—including the  $\alpha$ -fiber orientations between Goss and Bs—provoke an asymmetry of the ears of the cups, where the 0° cited “ears” are of greater height than the 90° “ears”. This asymmetry results in the formation of six ears, whereas in rare cases, two ears may appear. Hence, in order to achieve optimum properties for subsequent sheet-forming operations, a deep understanding of the evolution of texture during the production of the sheet is necessary [30]. In addition, the tensile properties of Al alloys are heavily influenced by the anisotropy, a parameter that is quantified through the r value [31]. Al alloys produced by means of cold rolling and annealing processes exhibit r values of the order of 0.55 to 0.85 [2]. The typical influences of rolling and recrystallization texture components on r values, as well as the {111}//ND components mentioned, are identified as relevant for increasing r values [26].

A number of models such as the Taylor/Bishop-Hill and Sachs are effectively utilized for the prediction of r values as well as earing behavior by taking into account texture data [32].

Nevertheless, the effect of the process stage that is examined in the present study on the texture versus mechanical properties (yield strength, tensile strength, elongation at fracture and R-values) has not been properly quantified yet for the examined rolling reduction percentages. Thus, the formation of well-balanced crystallographic texture leading to the desired properties is still a challenge for researchers [33].

The present study focuses on the effects of reduction (rolling) and heat treatment on the resulting crystallographic texture. Electron back-scatter diffraction (EBSD) and tensile tests are used to correlate microstructure and properties with the forming sequence and the thermal treatment background.

## 2. Materials and Methods

Three products were examined (Tables 1 and 2). Their details are as follows:

- A 2.8 mm thick, hot-rolled (h.r.) product (examined in the present paper in as-received state—as-rolled condition);
- Two cold-rolled (c.r.) sheets, a 1.3 mm (c.r.1) produced from h.r. and a 0.214 mm thick sheet (c.r.2) produced from c.r.1 without intermediate annealing (examined in the present paper in the as-received state and after laboratory annealing).

The 2.8mm thick hot-rolled product was examined in the as-received condition, whereas the 1.33 and 0.214 mm thick products were examined in both the as-received (cold-rolled) and heat-treated condition (annealed at 350 °C for 1 h). Annealing was conducted in the laboratory furnace.

**Table 1.** Description of examined samples.

Sample ID	Thickness (mm)	Condition
h.r.	2.8	Hot-rolled
c.r.1	1.3	Cold-rolled with 53% rolling reduction
c.r.a. 1	1.3	Cold-rolled with 53% rolling reduction and annealed
c.r.2	0.214	Cold-rolled 92% rolling reduction
c.r.a.2	0.214	Cold-rolled 92% rolling reduction and annealed

**Table 2.** Chemical composition of direct casted (DC) Al 5182 aluminum alloy.

Element	Si	Fe	Cu	Mn	Mg	Cr	Al
Wt%	0.11	0.21	0.04	0.35	4.60	0.01	Bal.

### 2.1. Metallographic Examination—Texture

Prior to the metallographic examination, all specimens were cut, in parallel to the rolling direction, before being cold mounted in resin. Specimens were afterwards grinded and polished by use of SiC papers as well as diamonds and silica suspensions. Metallographic examination was initially conducted by means of an optical microscope at a magnification range of 500×–1000× in order for the microstructure to be revealed and identified in the as polished condition. Through the observation of the samples in the optical microscope, an evaluation of the microstructure was undertaken in terms of a more general display of its characteristics (degree of recrystallization, direction of grains, etc.). Barker's electrolytic etch was afterwards applied in order for specimens to be examined in the etched condition as well according to references [33,34].

Through the utilization of a scanning electron microscope (SEM) FEI XL40 SFEG (current Thermo Fisher Scientific, Waltham, MA, USA), the microstructure of the samples was observed and qualitative elemental analysis of the particles at high magnification and the existence of secondary phases and measurement of average grain size were undertaken. Images of secondary electrons with a applied voltage of 20 kV at a working distance of 10 mm were obtained. The EDS technique was used to obtain atomic analysis spectra of some observed intermetallic phases.

The electron back-scatter diffraction (EBSD scans were collected employing a high-speed Hikari EDAX camera, EDEN Instruments SAS, Valence Cedex, France) electron diffraction microscopy technique provides quantitative data on the structure and crystallographic nature of compatible test specimens, making a significant contribution to the characterization of a microstructure. Specifically, EBSD determines the size and orientation of the grains, the crystallographic tissue, the nature of the grain boundaries, the phase identification in multiphase materials, as well as the distinction of submicroscopic structures. The above data are used to understand the relationships between microstructure characteristics and macroscopic properties so they are used for alloy design, material characterization and failure analysis.

For the EBSD analysis, the sample is placed inside the SEM in the as polished condition with a certain inclination of 70° relative to the incident electron beam. Voltage was set at 20 kV, while the step size was set at 0.1 μm to 1 μm depending on the material condition and the magnification utilized (100×–2000×) (examined areas 30 × 30 μm<sup>2</sup>–150 × 150 μm<sup>2</sup>). Working distance was set at 10 mm. Scanning data was then further analyzed by means of a post - processing software package in order for the various texture components to be identified and calculated.

### 2.2. Tensile Testing

Testing was performed on a tensile machine with a capacity of up to 30 kN as per the guidelines of ASTM E 646-00 [35] and ASTM E 517-00 [36] with parallel use of static extension meter according to the ISO 6892-1 standard at room temperature. Rolled lines were easily visible on the surface of the samples. The tensile specimens were produced by hydraulic pressing according to the specifications of the tensile test. Along the reduced cross-section, the specimens were characterized by a thickness of 0.4 mm, a width of 12.55 mm and a total length of 158 mm. In total, 3 tensile specimens were created to ensure repeatability. The bending specimens were cut with a cutting tool for thin rolled products. The specimens had dimensions of 2.5 × 5 mm<sup>2</sup>. A total of 45 specimens were produced [3 samples for each testing direction (0°, 45°, 90°) for each examined sample]. The standard deviation of all measurements was <1.5. In addition to the  $Rp_{0.2}$  yield strength, the tensile strength and the elongation at fracture, the anisotropy parameter  $r$  was also measured in all directions.

As for the anisotropy parameter  $r$ , the following are calculated for the three directions (0°, 45°, 90°), relative to the rolling direction according to Equation (1):

$$r = \frac{\ln \frac{w_1}{w_0}}{\ln \frac{t_1}{t_0}} \quad (1)$$

with  $w_0$  and  $t_0$  being the width and thickness of the tensile specimen in the gauge region prior testing, respectively. In addition,  $w_1$  and  $t_1$  are the width and thickness of the specimen in the same region just before necking occurs. It is noted that tensile testing speed was set at 10 mm/min throughout the test.

### 3. Results

The grain structure was revealed after Barker's etching. The hot rolled sample exhibited equiaxed grain structure. After the first cold roll pass, grains became elongated. After annealing, the grains retrieved their equiaxed morphology, which was retained even after the final cold roll pass. The final product showed a fully recrystallized microstructure (Figure 1).

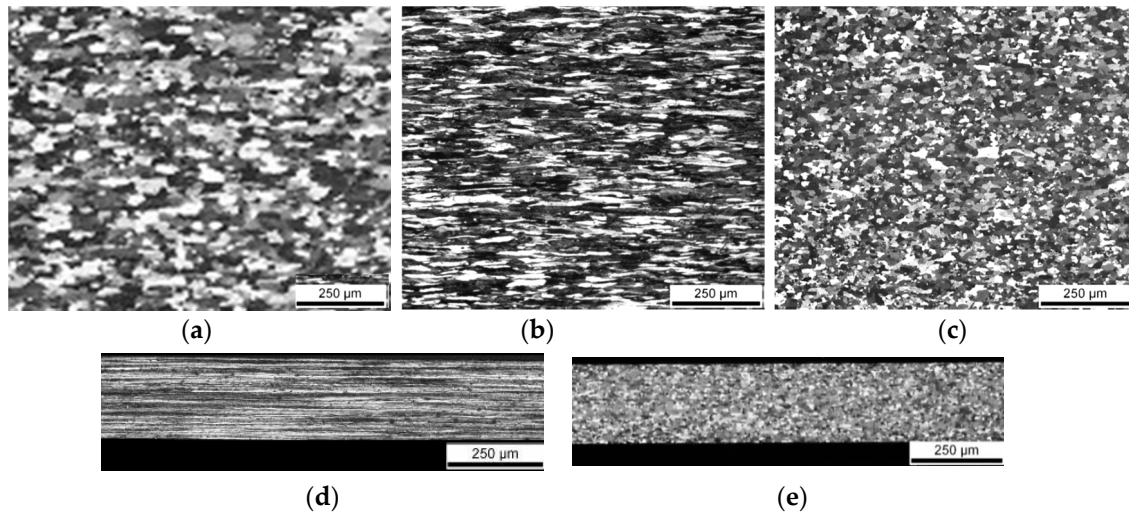


**Figure 1.** The microstructure of (a) hot-rolled sheet, (b) cold-rolled 1.3 mm sheet, (c) cold-rolled 1.3 mm annealed sheet, (d) cold-rolled 0.214 mm sheet and (e) cold-rolled 0.214 mm annealed sheet after Barker's etching.

Second phase particles of  $Al_6(Mn, Fe)$  and  $Mg_2Si$  are dispersed all over the matrix of the examined samples. Indicative SEM micrographs of the particle dispersion in the matrix of h.r. and c.r.2 samples are shown in Figure 2.

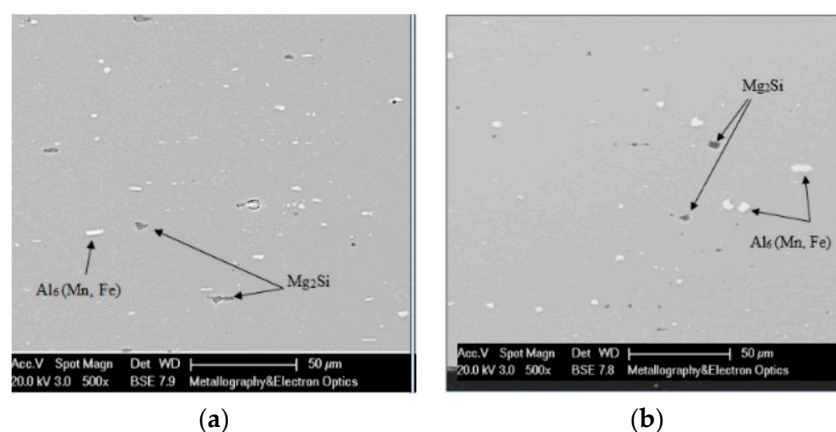


**Figure 2.** Scanning electron microscopy (SEM) images showing (a) h.r. sample and (b) c.r.2.

Intensities from inverse pole figure (IPF) and pole figure (PF) diagrams are related with the texture intensity of the examined sample. Red color indicates the points, where the highest texture intensity is observed. The lower intensity indicates higher isotropy of the texture and, consequently, the higher isotropy of mechanical properties as well. PF and IPF diagrams exhibit the same information from a different aspect. The findings originating from EBSD data are graphically illustrated in Figure 3:

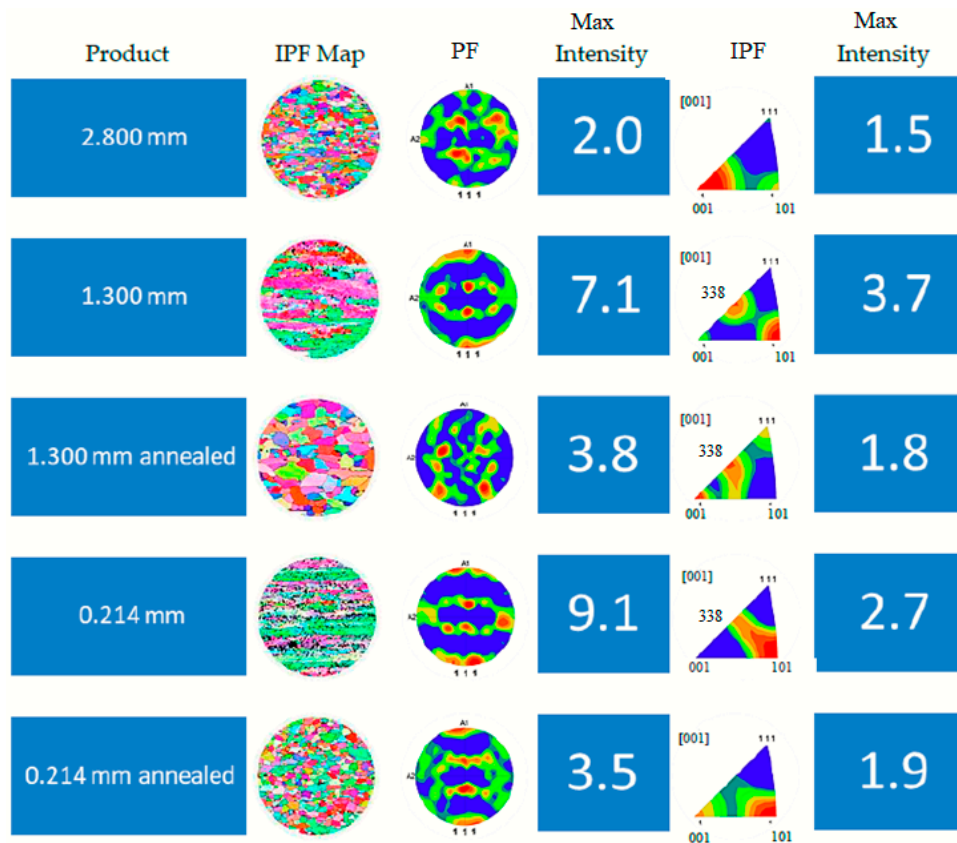


Figure 3. Electron back-scatter diffraction (EBSD) data for the examined products.

Figure 3 presents the IPF maps and microstructures as well as the PF for each product examined. The relevant intensities are also presented on the right side of Figure 3. The h.r. sample is partially recrystallized showing a typical hot-rolled PF exhibiting relatively low texture intensity (2.0 in the PF diagram and 1.5 in the IPF diagram). After 53% thickness reduction, sample c.r.1 grains tend to be more elongated, while the IPF diagram indicates a shift towards {111} orientation with measured intensity 7.1 and 3.7 for PF and IPF diagrams respectively. The annealing creates a fully recrystallized and equiaxed grain structure, while the intensity is low (3.8 and 1.8 in the PF and the IPF diagram respectively). At the same time, a crucial difference is observed from the h.r. to the c.r.a.1 sample: a weak {111} and a strong {338} component is formed. After the final cold pass, the higher amount of texture intensity has been measured (9.1 in the PF and 2.7 in the IPF diagram respectively) (Figures 3 and 4). After the final annealing, the texture intensity reaches similar values with the ones measured on the c.r.a.1 sample (3.5 and 1.9 in the PF and in the IPF diagram respectively) (see Figure 3). At c.r.a.2 the {001} had been reformed after been seen in h.r. and in c.r.a.1.

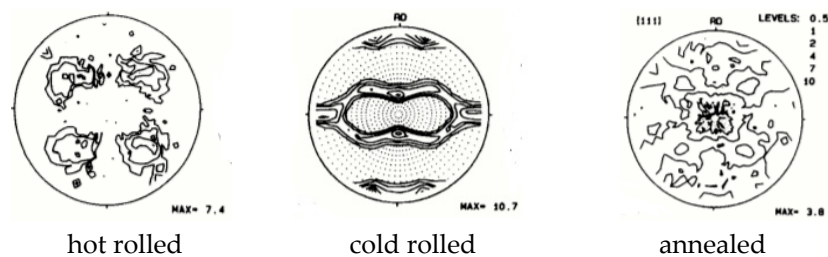
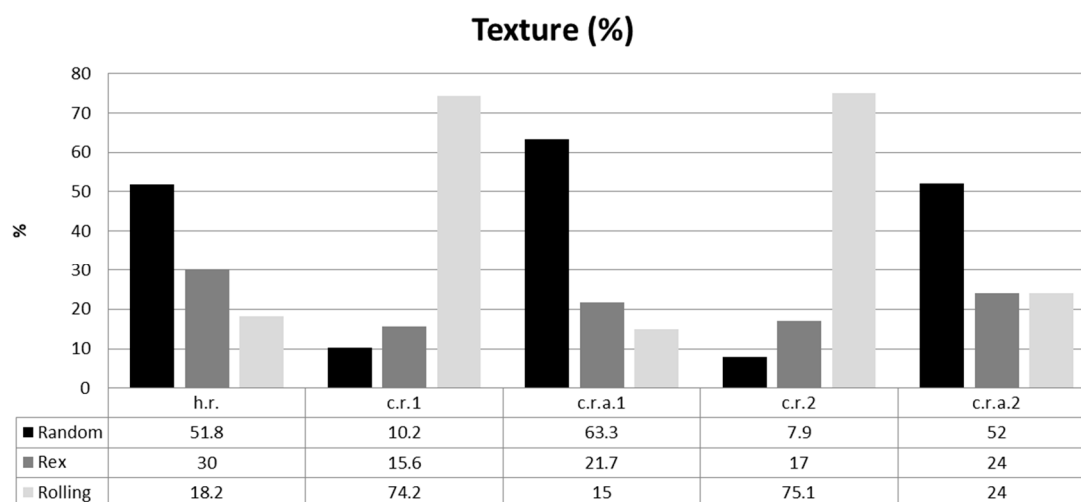


Figure 4. Typical textures [(111) pole figures] in different processing stages of Al-alloy sheet [32].

For reference, the typical appearance of PF in relation to the rolling process and heat treatment applied are given in Figure 4 [37].

The Al sheet texture exhibits three main categories of component, recrystallization (cube, P, R), rolling (brass, copper, Goss, S, Dilamore or Taylor) and shear (rotated cube, inverse brass, E, F) texture components. The h.r. sample, mostly exhibited recrystallization texture accompanied by a significant amount of rolling texture (Figure 5). The main components detected in this state are Q, R and brass. After 52.5% thickness reduction, the rolling texture increased and the main components detected are R and Goss from the remained texture recrystallization and intense S, brass, copper and Taylor.



**Figure 5.** Texture percentage chart.

The effect of annealing changed the components analogies increasing the random texture. Q, R and Goss increased leaving just a small amount of S and Taylor from the previous deformation. The final pass of 92% thickness reduction led to the formation of high amounts of S and brass, followed by Taylor and Copper. The representative recrystallization component is R. The ultimate annealing process provoked the formation of a high amount of R coexisting with brass and S (see Figure 5). Cold rolling of the h.r. sample, led to an increased amount of both rolling and recrystallization texture percentage for the c.r.1 and c.r.2 samples. It also led to increased anisotropy (see the increased intensities PF and IPF diagrams). Annealing treatment formed low PF and IPF intensities, which resemble to the original h.r. sample observed intensities.

The random texture of both annealed sheet samples increased significantly reinforcing the isotropic behavior of these materials with approximately 1% normal anisotropy. This could be explained by the fact that in c.r.a.1 the nucleation of the cube component was inadequate ( $r$ -CubeRD) and the amount of recrystallization texture was higher than the remaining deformation texture. In contrast the c.r.a.2 exhibited greater volume fractions of the cube and R components, which favor the earing formation of  $0/90^\circ$  ears. In both cases the recrystallization texture in the annealed samples is higher than the cold-rolled samples before.

EBSD findings are analytically presented in the following chart, where the exact percentages of the random, recrystallization (Rex) and rolling texture are shown for each examined case (Figure 5).

The mechanical properties after annealing for both cold-rolled products exhibited significant similarity with regard to the h.r. mechanical properties. Tensile testing results are given in Figures 6–8. In particular h.r. exhibited yield strength of 139 MPa at  $0^\circ$ , of 144 at  $45^\circ$  and of 145.5 at  $90^\circ$  whereas c.r.a.1 showed 155 MPa, 148.5 MPa and 154.5 MPa and c.r.a.2 161 MPa, 152.5 MPa and 160.5 MPa, respectively. Concerning the tensile strength, h.r. exhibited 301.5 MPa at  $0^\circ$ , 298 MPa at  $45^\circ$  and 299.5 MPa at  $90^\circ$  while c.r.a.1 showed 312.5 MPa, 303 MPa and 301.5 MPa and c.r.a.2 311.5 MPa, 298.5 MPa and 303 MPa, respectively. The measured values of the h.r, c.r.a.1 and c.r.a.2 confirmed that regarding the yield strength and the tensile strength, the annealing temperature restored the mechanical properties after the deformation, but did not have such an intense impact on crystallographic components (see Figure 3).

The PF intensity was selected as an indicator of intense texture presence and, therefore, less isotropic behavior.

Yield strength and tensile strength increased to an analogous extent in all directions after cold rolling and decreases after annealing (Figures 6 and 7). The 0° direction exhibited slightly higher strength values compared to the other directions for all but the 2.8 mm thick products.

In both annealed cases (c.r.a.1 and c.r.a.2) the elongation at fracture was increased which can be related to the reduction of dislocation density and the new formed grain size and morphology (Figure 8).

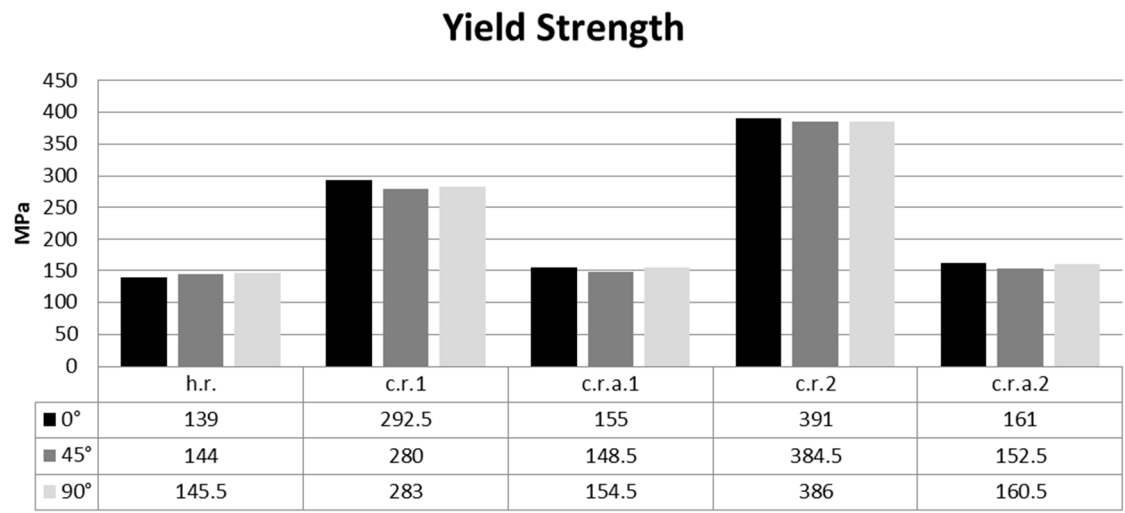


Figure 6. Yield strength data for all products and conditions.

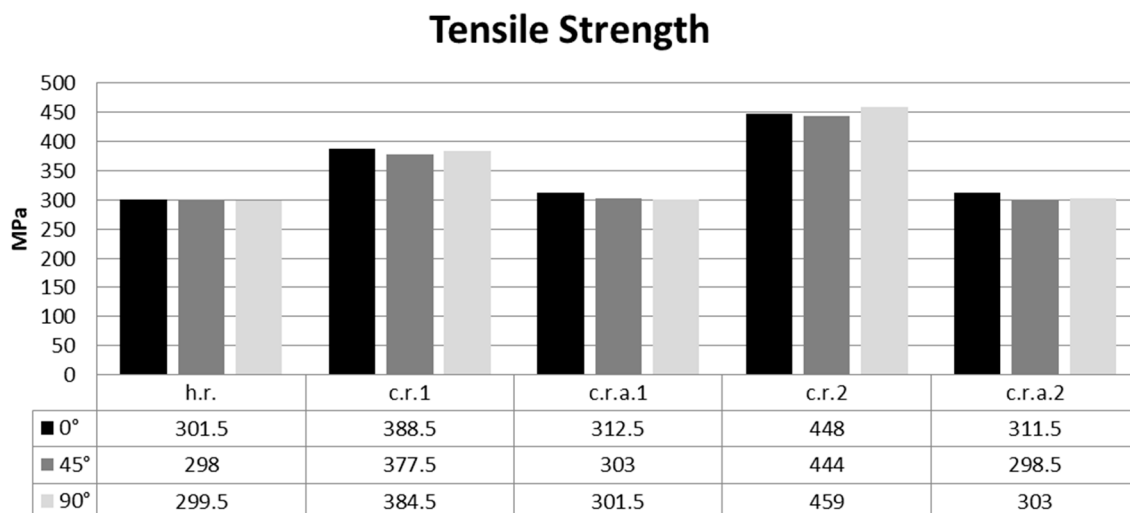


Figure 7. Tensile strength data for all products and conditions.

### Elongation at fracture

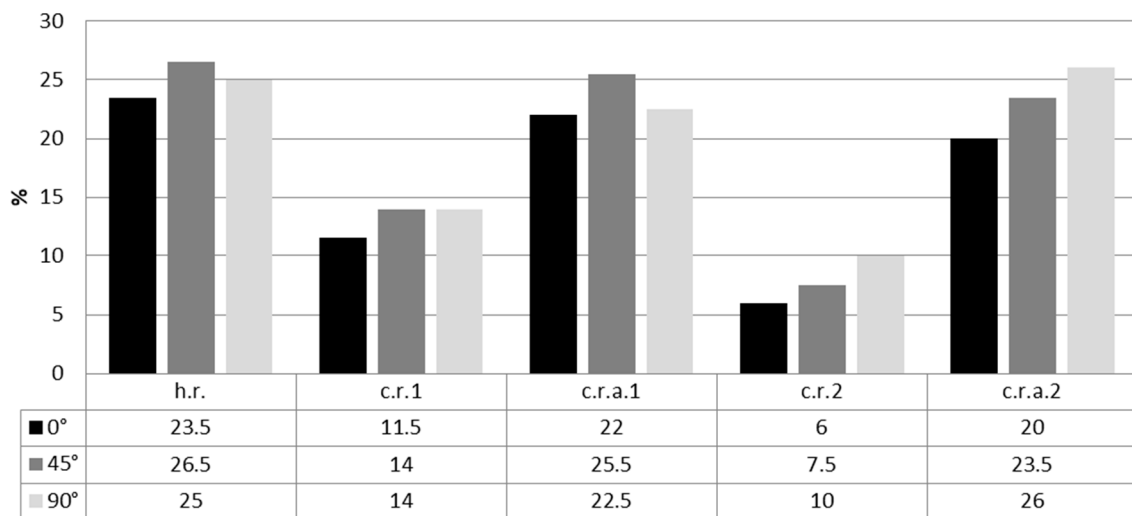


Figure 8. Elongation at fracture data for all products and conditions.

On a similar note, the r value was also influenced as a result of the various processing steps. In particular, cold rolling resulted into a reduction of the 0° r value in the rolling direction, whereas a significant increase was noted in the 45° and 90° directions. Similar observations were made for the 1.33 and 0.214 mm thick cold-rolled products. Annealing resulted in an increase of the r value in the rolling direction, whereas the r values in the 45° and 90° directions decreased. As a result, all r values after annealing closely resembled the relevant values of the original h.r. sample (see Figure 9). Sample c.r.1 after 53% thickness reduction, exhibited decreased elongation (<14%). After the annealing process, elongation increased to >22%, which dropped to <10% after 92% reduction. After the final annealing, elongation reached along all the 0°, 45° and 90° directions, respectively >20%.

### r value

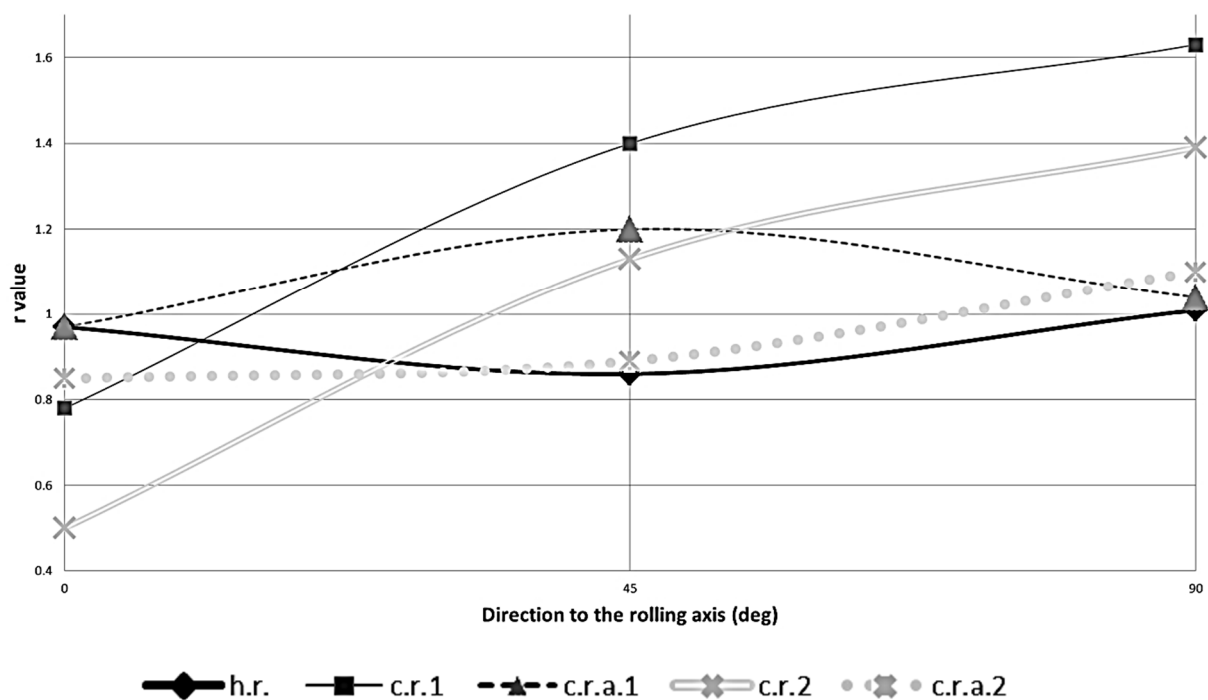


Figure 9. The r average in relation to direction (0°, 45°, 90°).

#### 4. Discussion

The hot-rolled sheet exhibited a balanced amount of rolling and recrystallization texture components along with random texture. Cold rolling of the 2.8 mm hot-rolled sheet led to an increased amount of rolling texture, at the expense of both random and recrystallization textures. The effect of annealing was evident through the reduction of the rolling and recrystallization components percentages, whereas the random texture percentage increased. The amount of rolling texture components decreased whereas the amount of recrystallization and random components increased.

Cold rolling of the original 2.8 mm thick sheet resulted in increased anisotropy as indicated by the increased intensities PF and IPF diagrams. In contrast, post-cold-rolling annealing resulted in low PF and IPF intensities indicating a behavior relating to a more isotropic material, comparable to the original 2.8 mm thick hot-rolled product. This is beneficial due to the increase of fracture elongation and the reduction of anisotropy and elongated grain morphology, which can assume increased formability. In addition, cold rolling resulted in increased yield and tensile strength values as well as a significant decrease of fracture elongation due to the presence of fibrous grain with increased anisotropy. The dislocation density and grains size and morphology have major effects on elongation at fracture of the tensile specimens. PF intensity controls anisotropy of those mechanical properties, but hardly their overall level.

This effect was more pronounced in the 0.214 mm thick product that had to undergo two reductions instead of a single one, as was the case for the 1.33 mm thick product. Post cold rolling annealing restored the mechanical properties of the two cold-rolled products in levels comparable to the 2.8 mm thick hot-rolled product and as a result elongation and formability were improved. Cold rolling texture is transformed to the cube component during annealing, which favors its performance with regards to bending, whereas the addition of  $\{111\}\langle uvw \rangle$  components such as  $\{111\}\langle 110 \rangle$  during annealing favors deep drawability.

The random texture of both the annealed sheet samples was increased significantly which could be understood due to the suppression of nucleation and subsequent growth of the cube orientation which is expected to be strong in recrystallized aluminum rolled products. The almost homogeneous  $r$  value of the h.r., c.r.a.1 and c.r.a.2, a better formability could be expected [37].

Suitable texture control relating to specific applications is required for the improvement of sheet metal behavior with regards to further forming operations (e.g., bending and deep drawing).

Structural variables could be used in measurements of dislocation cell morphology and material behavior. Therefore, the dependence of the cell morphology should be identified from the thermomechanical processes upon crystallite lattice orientation. Nevertheless the scan of areas of the order of a few  $\mu\text{m}$  or mm requires small step sizes in the case of highly deformed samples that exhibit good statistical accuracy, however, according to relevant literature [4–8]. As such, data obtained from automated EBSD analysis of highly deformed microstructures can lead to a deeper understanding of the deformation behavior and the recrystallization and microstructure evolution sequences with regards to the applied deformation steps. Thus, the final microstructure and mechanical properties can be tailored accordingly with regard to the final thickness and the required strength levels as well as the necessary subsequent formability, which is the ultimate case.

EBSD data showed that after the first cold roll pass (c.r.1), crystallographic texture mainly contains  $\beta$  fiber texture (which was present even from the hot rolling process) with strong Taylor component. After annealing treatment, texture evolved mainly to Q, R and weak  $\beta$  fiber texture with the Taylor component maintaining the highest intensity. The second and final pass evolved the observed texture into a mixture of  $\beta$  fiber texture with the S component having the highest intensity and simultaneously strong Goss component; no significant cube texture was found. A possible path between directions  $\{101\}$  and  $\{338\}$ , could be a way for the nucleation of cube crystallographic components. At c.r.a.2 the  $\{001\}$  had been reformed after being seen in h.r. and in c.r.a.1.

Recrystallization exhibits characteristics of phase transformation in which the replacement of deformed material due to the creation of nuclei and growth of recrystallized grains can lead to

significant changes of the resulting texture. The latter does not lead to precise orientation relationships among deformed and recrystallized material, contrary to the phase transformations. It should be stated that recrystallization does not always lead to texture transformations, especially when large volume fractions of second phase particles are present or when the deformation was axisymmetric.

The quantitative correlation between PF intensity and mechanical properties could be attributed to the anisotropy increase that takes place after each mechanical process, but it is important to observe the analogy of these values towards texture. The impact of texture components is strong on the variations of  $r$ -value for different directions. In all examined cases, the texture component occupies >92% of the total volume fraction of grains. The remaining volume fraction is populated by randomly oriented grains. The  $r$ -value is non-uniform for all the examined direction for each sample. It is clearly seen from Figure 9 that the optimal texture for the smallest possible in-plane anisotropy clearly gives an average  $r$ -value less than 1.0 (exhibited by h.r.).

The  $r$  values of the Al sheet, when measured after hot rolling, can be regarded as more appropriate amongst those of all measured samples. After annealing of the 92% reduced sheet,  $r$  measurements indicated a quite good forming behavior, but the effect of the final pass towards the anisotropy and  $r$  values at  $0^\circ$ ,  $45^\circ$  and  $90^\circ$  could not be eliminated throughout annealing. A higher, than expected for this Al alloys,  $r$  value was observed at  $90^\circ$ , a behavior that can be attributed to the higher amount of rolling texture and especially to the presence of the S component. Therefore, a reduced amount of thickness reduction, the number of rolling passes and the lubrication could provoke better results and, possibly, the ideal percentage of rolling and annealing crystallographic components.

## 5. Conclusions

This work demonstrates that the mechanical properties of Al5182 can be influenced by the deformation sequence as well as the subsequent annealing conditions. Moreover, texture is especially important with regards to formability, especially for the deep drawing of thin sheets.

More specifically:

- After the application of the various rolling steps as well as the appropriate heat treatment ( $350^\circ\text{C}$  for 1 h), even in the material that was submitted to 92% thickness reduction (c.r.2-0.214 mm), sheets exhibited an increase of yield and tensile strength, mechanical properties closely resemble those of the reference material (as-received condition after hot rolling, h.r.). The formation of  $\{110\}$ //RD texture components in h.r. favors the increase of the elongation of the alloy. In addition the relevant PF and IPF intensities increased after thickness reduction as a result of increased anisotropy. This is also evident by the recorded  $r$  values, which are heavily influenced by cold rolling whereas after the annealing process they are restored to the as-received product levels. The same applies for the tensile properties and the intensities of the PF and IPF diagrams.
- The initial texture (formed from hot rolling) has a strong influence on the distribution of component intensities along the  $\beta$  fiber. The  $\beta$ -fiber maximum intensity was lower than 10, revealing a low yet remaining amount of rolling texture in the material after the intermediate annealing. Equivalence among rolling and recrystallization crystallographic components is essential to retain formability and toughness in order to form a fine and equiaxed grain structure.
- To increase the  $r$  value towards all directions, R orientation  $[123]\langle 634 \rangle$  is expected to be most efficient, but this orientation shows a low  $r$  value of about 0.8 mainly at the  $0^\circ$  and  $45^\circ$  directions. Therefore, the Goss orientation  $[011]\langle 100 \rangle$ , which also increases the  $r$  value must be developed to some extent.  $[001]\langle uvw \rangle$  textures such as the cube orientation are non-preferable with regard to the improvement of the  $r$  value. The variations observed in the products that have been annealed were coherent with the R texture component. The  $r$ -value of the as-rolled material was consistent with the presence of cold-rolling texture components.

**Author Contributions:** Conceptualization, E.G., S.P. (Spyros Papaefthymiou); Methodology, E.G., S.P. (Spyros Papaefthymiou), S.P. (Sofia Papadopoulou); Software, S.P. (Sofia Papadopoulou) and A.K.; Validation, S.P. (Sofia Papadopoulou); Formal Analysis, S.P. (Sofia Papadopoulou), E.G. and A.K.; Investigation, A.K. and S.P. (Sofia Papadopoulou); Resources, S.P. (Spyros Papaefthymiou); Data Curation, S.P. (Sofia Papadopoulou) and A.K.; Writing—Original Draft Preparation, S.P. (Sofia Papadopoulou) and A.K.; Writing—Review & Editing, E.G. and S.P. (Spyros Papaefthymiou); Visualization, S.P. (Sofia Papadopoulou); Supervision, E.G. and S.P. (Spyros Papaefthymiou); Project Administration, S.P. (Sofia Papadopoulou). All authors have read and agreed to the published version of the manuscript.

**Funding:** This research received no external funding.

**Acknowledgments:** The authors would like to express their gratitude to ELKEME SA and ELVAL SA managements for all the kind support. Pantazopoulos, Vazdirvanidis are highly appreciated for the fruitful discussions and Toulfatzis for the mechanical testing.

**Conflicts of Interest:** The authors declare no conflict of interest. The funders had no role in the design of the study; in the collection, analyses, or interpretation of data; in the writing of the manuscript; or in the decision to publish the results.

## References

- Hatch, E. *Aluminum: Properties and Physical Metallurgy*; ASM International: Almere, The Netherlands, 1984; pp. 134–199. [[CrossRef](#)]
- Cantor, B.; Grant, P.; Johnston, C. *Automotive Engineering: Lightweight, Functional, and Novel Materials*; Taylor and Francis: Abingdon, UK, 2008.
- Bunge, H.J. *Texture Analysis in Materials Science*; Butterworths: London, UK, 1982.
- Liu, J.; Morris, J.G. Recrystallization microstructures and textures in AA 5052 continuous cast and direct chill cast aluminum alloy. *Mater. Sci. Eng. A* **2005**, *385*, 453–454. [[CrossRef](#)]
- Yu, X.F.; Zhao, Y.M.; Wen, X.Y.; Zhai, T. A study of mechanical isotropy of continuous cast and direct chill cast AA5182 Al alloys. *Mater. Sci. Eng. A* **2005**, *394*, 376–384. [[CrossRef](#)]
- Bunk, W.; Lucke, K.; Masing, G. Rolling and recrystallization textures of aluminum. *Z Metallkd* **1954**, *45*, 584–593.
- Lücke, K. Rolling and recrystallization texture of aluminum. Texture of cold-rolled aluminum. *Z Metallkd* **1954**, *45*, 86–92.
- Romhanji, E.; Popovic, M.; Glisic, D.; Stefanovic, M.; Milovanovic, M. On the Al-Mg alloy sheet for automotive applications: Problems and solutions. *Metallurgija* **2004**, *10*, 202–216.
- Davis, J.R. *Alloying: Understanding the Basics*; ASM International: Novelty, OH, USA, 2001.
- Hirsch, J. Texture and anisotropy in industrial applications of aluminium alloys. *Arch. Metall. Mater.* **2005**, *50*, 21–34.
- Miller, W.S.; Zhuang, L.; Bottema, J.; Wittebrood, A.J.; De Smet, P.; Haszler, A.; Vieregge, A. Recent development in aluminium alloys for the automotive industry. *Mater. Sci. Eng. A* **2000**, *280*, 37–49. [[CrossRef](#)]
- Alharthi, N. Microstructure Evolution of Asymmetrically Rolled AA-5182. In Proceedings of the ASME District A 2011 Student Professional Development Conference, Philadelphia, PA, USA, 2 June 2011.
- Bate, P.; Oscarsson, A. Deformation banding and texture in hot rolled Al–1.0Mn–1.2Mg alloy. *Mater. Sci. Technol.* **1990**, *6*, 520–527. [[CrossRef](#)]
- Humphreys, F.J.; Hatherly, M. *Recrystallization and Related Annealing Phenomena*; Elsevier: Amsterdam, The Netherlands, 2004.
- Hirsch, J.; Al-Samman, T. Superior light metals by texture engineering: Optimized aluminum and magnesium alloys for automotive applications. *Acta Mater.* **2013**, *61*, 818–843. [[CrossRef](#)]
- Kim, K.J.; Won, S.-T.; Park, J.-H. Texture analysis of 5182 aluminum alloy sheets for improved drawability by rolling process. *Mater. Werkst.* **2012**, *43*, 373–378. [[CrossRef](#)]
- Theis, H. *Handbook of Metalforming Processes*; CRC Press: New York, NY, USA, 1999.
- Zhang, L.; Wang, Y.; Yang, X.; Li, K.; Ni, S.; Du, Y.; Song, M. Texture, microstructure and mechanical properties of 6111 aluminum alloy subject to rolling deformation. *Mater. Res.* **2017**, *20*, 1360–1368. [[CrossRef](#)]
- Kocks, U.F.; Tome, C.N.; Wenk, H.R. *Texture and Anisotropy*; Cambridge University Press: Cambridge, UK, 2000.
- Engler, O.; Vatne, H.E.; Nes, E. The roles of oriented nucleation and oriented growth on recrystallization textures in commercial purity aluminium. *Mater. Sci. Eng. A* **1996**, *205*, 187–198. [[CrossRef](#)]

21. Bennett, T.A.; Sidor, J.; Petrov, R.H.; Kestens, L.A. The effect of intermediate annealing on texture banding in aluminum alloy 6016. *Adv. Eng. Mater.* **2010**, *12*, 1018–1023. [[CrossRef](#)]
22. Totten, G.E.; Funatani, K.; Xie, L. *Handbook of Metallurgical Process Design*; Marcel Dekker Inc.: New York, NY, USA, 2004.
23. Kim, H.-W.; Lim, C.-Y. Annealing of flexible-rolled Al–5.5wt%Mg alloy sheets for auto body application. *Mater. Des.* **2010**, *31*, S71–S75. [[CrossRef](#)]
24. Okada, M.; Hirano, S. Effect of Annealing Condition on Earing and Texture Formation in Cold Rolled AA5182 Aluminum Alloy. In Proceedings of the 13th International Conference on Aluminum Alloys (ICAA13), Pittsburgh, PA, USA, 25 June 2012.
25. Liu, W.C.; Zhai, T.; Man, C.-S.; Morris, J.G. Quantification of recrystallization texture evolution in cold rolled AA 5182 aluminum alloy. *Scr. Mater.* **2003**, *49*, 539–545. [[CrossRef](#)]
26. Liu, W.C.; Morris, J. Effect of initial texture on the recrystallization texture of cold rolled AA 5182 aluminum alloy. *Mater. Sci. Eng. A* **2005**, *402*, 215–227. [[CrossRef](#)]
27. Leffers, T.; Ray, R. The brass-type texture and its deviation from the copper-type texture. *Prog. Mater. Sci.* **2009**, *54*, 351–396. [[CrossRef](#)]
28. Barrett, C.S. *The Structure of Metals*, 2nd ed.; McGraw-Hill: New York, NY, USA, 1952.
29. Hutchinson, W.B.; Ekström, H.E. Control of annealing texture earing in non-hardenable aluminum alloys. *Mater. Sci. Technol.* **1990**, *6*, 1103–1112. [[CrossRef](#)]
30. Engler, O. Simulation of rolling and recrystallization textures in aluminium alloy sheets. *Mater. Sci. Forum* **2007**, *550*, 23–34. [[CrossRef](#)]
31. Savoie, J.; Jonas, J.J.; MacEwen, S.R.; Perrin, R. Evolution of r-value during the tensile deformation of aluminium. *Textures Microstruct.* **1995**, *23*, 149–171. [[CrossRef](#)]
32. Jamaati, R.; Toroghinejad, M.R. Effect of alloy composition, stacking fault energy, second phase particles, initial thickness, and measurement position on deformation texture development of nanostructured FCC materials fabricated via accumulative roll bonding process. *Mater. Sci. Eng. A* **2014**, *598*, 77–97. [[CrossRef](#)]
33. Voort, G.F.V. *Metallography, Principles and Practice*; McGraw-Hill: New York, NY, USA, 1984.
34. ASTM. *E407-07 (2015) Standard Practice for Microetching Metals and Alloys*; ASTM International: West Conshohocken, PA, USA, 2015.
35. ASTM. *E646-00: Standard Test Method for Tensile Strain-Hardening Exponents (n-Values) of Metallic Sheet Materials*; ASTM International: West Conshohocken, PA, USA, 2000.
36. ASTM. *E517-00: Standard Test Method for Plastic Strain Ratio r for Sheet Metal*; ASTM International: West Conshohocken, PA, USA, 2000.
37. Hirsch, J.R. Aluminium alloys for automotive application. *Mater. Sci. Forum* **1997**, *142*, 33–50. [[CrossRef](#)]

**Publisher’s Note:** MDPI stays neutral with regard to jurisdictional claims in published maps and institutional affiliations.



© 2020 by the authors. Licensee MDPI, Basel, Switzerland. This article is an open access article distributed under the terms and conditions of the Creative Commons Attribution (CC BY) license (<http://creativecommons.org/licenses/by/4.0/>).